Copper-based nanocatalysts for 2-butanol dehydrogenation: Screening and optimization of preparation parameters by response surface methodology

Elham Geravand*, Zahra Shariatinia*,†, Fereydoon Yaripour*, and Saeed Sahebdelfar**

*Department of Chemistry, Amirkabir University of Technology, P. O. Box 15875-4413, Tehran, Iran
**Catalysis Research Group, Petrochemical Research & Technology Company,
National Iranian Petrochemical Company, P. O. Box 1493, Tehran, Iran

Abstract−Two types of copper-based dehydrogenation nanocatalysts (Cu/ZnO/Al$_2$O$_3$ and Cu/SiO$_2$) were prepared from various precursors by impregnation (IM), sol-gel (SG) and co precipitation (COPRE) methods. The structures of samples were characterized by N$_2$ adsorption-desorption, XRD, XRF, TPR, N$_2$O-Titration, FT-IR, FE-SEM and TEM techniques. The catalytic performance tests in vapor-phase dehydrogenation of 2-butanol to methyl ethyl ketone (MEK) were carried out in a fixed-bed reactor at a temperature of 260 °C under atmospheric pressure and LHSV of 4 mL/(h·g cat). The experimental results indicated that (i) the copper oxide over the COPRE nanocatalyst was reduced at a lower temperature (222 °C) in comparison with the CuO reduced on the SG and IM samples (243 and 327 °C, respectively). Also, the percentage of reduction of CuO species on COPRE catalyst was the highest (98.8%) in comparison with the two other samples, (ii) the COPRE nanocatalyst exhibited the highest activity for the dehydrogenation of 2-butanol to MEK, and (iii) co-precipitation method was selected as an optimum method for preparation of nanocatalyst. The central composite experimental design method was applied for investigation of the effects of four critical preparation factors on the MEK selectivity of Cu/ZnO/Al$_2$O$_3$ nanocatalyst. The results showed that Cu/Zn molar ratio and precipitation pH are the most effective factors on the response and the optimum conditions for synthesis of Cu/ZnO/Al$_2$O$_3$ nanocatalyst with maximum selectivity of MEK were T$_{(pre)}$=67.5 °C, T$_{(aging)}$=68.8 °C, pH$_{(pre)}$=7.27 and Cu/Zn molar ratio=1.38. The performance of the prepared nanocatalyst at the optimum conditions was comparable to the commercially available nanocatalyst.

Keywords: Copper Nanocatalyst, 2-Butanol, Dehydrogenation, Methyl Ethyl Ketone (MEK), Response Surface Methodology (RSM)

INTRODUCTION

Methyl ethyl ketone (MEK) is an industrial organic solvent that is characterized by its suitable boiling point, good solubility, volatilization, stability and nontoxic nature. It is applied as a solvent in paints, dyes, adhesives (especially for PVC pipes), magnetic tapes, pharmaceutical and refining industries. MEK also is used as a solvent for fats, oils, waxes and resins. It is also an important raw material for the production of methyl ethyl ketone peroxide [1,2]. As per 2012, the global production of MEK reached 1,141 thousand metric tons (2.5 billion pounds). The global demand for MEK was 1,100 thousand metric tons (2.4 billion pounds). Demand for MEK has increased at a rate of 6.5% per year and continues to grow at about this rate. The percentage sales distribution for MEK is as follows: (a) paint, lacquers, printing inks-40%, (b) chemical industry-18% and (c) miscellaneous-42%. There are a few processes for the production of MEK such as (1) vapor phase dehydrogenation of 2-butanol, (2) liquid phase oxidation of n-butane, (3) direct oxidation of *n*-butane (Hoechst-Wacker process) and (4) direct oxidation of *n*-butane (Maruzen process). Currently, most of MEK (88%) is

commercially produced by dehydrogenation of 2-butanol, which is an exothermic reaction (51 kJ/kmol). Although MEK is not a hazardous air pollutant, it is a volatile organic compound (VOC); considerable measures are taken to prevent its release to the atmosphere. Thus, processes and equipment for manufacture, transfer and storage are continuous and enclosed. The remaining MEK is produced by a process in which liquid butane is catalytically cracked, giving both acetic acid and MEK. This process gives high conversion of 2-butanol, high selectivity to MEK, improved yield with longer catalyst life and easier product separation compared with other processes. A two-step process from *n*-butylenes is used in which butylenes are first hydrated to give secondary butyl alcohol (SBA or 2-butanol), and subsequently dehydrated to MEK in vapor phase. The main products of the reaction are MEK and hydrogen [3-9].

The commercial alcohol dehydrogenation catalysts are copper, brass or zinc-based [3,10,11]. Copper-based catalysts are found to be quite effective in dehydrogenation of 2-butanol due to their lower operation temperatures and minimum side reactions [3,10]. Copper-based catalysts can be either unsupported or supported, the latter being more common. The support provides a large surface area for the copper to be deposited on. Unsupported copper catalysts have much lower surface areas. The activity of the catalyst is usually proportional to the surface area of the active phase, and thus a large copper surface area will yield a more active catalyst [1-

†To whom correspondence should be addressed.
E-mail: shariati@aut.ac.ir

4,10,12-16]. Fang et al. synthesized a series of mesoporous Cu-Zn-Al_2O_3 catalysts using precipitation method under the same preparation conditions (pH=9, and NaOH (2 M) as the precipitator under ambient temperature) and the catalytic performance of the meso-structured Cu-Zn-Al_2O_3 samples was compared with the catalyst prepared by general co-precipitation procedure [4]. They found that the mesoporous Cu-Zn-Al_2O_3 catalysts were more active in the formation of MEK with lower by-products formation compared with the catalysts made by the co-precipitation method. Note that meso-structured catalysts are expensive materials due to their precursors, and their high prices limit their applications in industrial scale. On the other hand, the cost of CuO/ZnO/Al_2O_3 catalyst prepared using co-precipitation method is much lower than meso-porous Cu-Zn-Al_2O_3 catalyst. Keuler et al. investigated the effect of support type (SiO_2 and MgO) for copper-based catalysts prepared by wet impregnation on their performance in MEK production through dehydrogenation reaction [3]. They established that the MgO supported catalysts showed low MEK yields because of their low BET surface areas, but the highest MEK yields were achieved using silica supported catalysts with an optimum copper loading on the support (15 wt%).

Along with the expanding demand for MEK, increasing interest has been devoted to synthesizing new catalytic systems. Doped-ZnO with indium and nitrogen was used as a catalyst in 2-buta-nol conversion. It was found that $(Zn_{1-z}In_z)(O_{1-x}N_x)$ materials show high conversion and yield toward MEK without any electron acceptors [17]. The synergetic effects between SnO_2 and MoO_3 in the catalytic dehydrogenation of 2-butanol to MEK were studied in the presence of oxygen [18]. The iron/calcium-hydroxyapatite catalysts containing different amounts of iron-Fe(x)/CaHAp prepared by cation exchange in aqueous media were also examined [19]. The Fe(x)/CaHAp catalysts were found to be active in butan-2-ol conversion. Increasing the iron content enhanced the acid properties of the catalysts and decreased the dehydrogenation activity.

The aim of this work was to study the influences of the preparation method and reaction conditions on the catalytic properties of copper-based nanocatalysts in dehydrogenation of 2-butanol to MEK. The prepared samples were characterized with a variety of surface and bulk techniques including BET, XRD, XRF, TPR, N_2O-Titration, FT-IR, FE-SEM and TEM analyses. Central composite design (CCD) as a division of the response surface method (RSM) was applied to predict the optimum synthetic conditions for the selected nanocatalyst to obtain the maximum selectivity of MEK (S_{MEK}).

EXPERIMENTAL METHODS

1. Materials

The starting materials were copper hydroxide carbonate [Cu_2-$CO_3(OH)_2$, 97.5 wt%, industrial grade], zinc oxide [ZnO, 99.7 wt%, industrial grade], aluminum nitrate nanohydrate [$Al(NO_3)_3\cdot9H_2O$, 97 wt%, industrial grade], nitric acid [HNO_3, 56 wt%, Industrial grade], sodium carbonate [Na_2CO_3, 99.4 wt%, industrial grade], tetraethyl *ortho*-silicate [TEOS, $Si(OC_2H_5)_4$, 98 wt%, Merck], oxalic acid [$H_2C_2O_4$, 99.5 wt%], ethanol [C_2H_5OH, 99 wt%, Merck], sodium hydroxide [NaOH, 99.6 wt%, Merck] and amorphous silica sup-

port [supplied from Sasol Company].

2. Catalyst Synthesis

Three different methods were used to prepare two kinds of copper catalysts. The nanocatalyst prepared by co-precipitation has the general form as CuO/ZnO/Al_2O_3, whereas those prepared by impregnation and sol-gel methods have the general form as CuO/SiO_2. The compositions of nanocatalysts were chosen based on analyzing the structures of commercial catalysts supplied by Sasol Company and Fushun Research Institute of Petroleum & Petrochemicals and named as CCS and CCFRI, respectively.

3. Co-precipitation Method

Solution A was prepared by mixing 1 M solution of the precursors (225 mL copper nitrate, 200 mL zinc nitrate, 75 mL aluminum nitrate) and solution B (650 mL) was a 1 M sodium carbonate solution. The precipitation was carried out by simultaneous addition of the nitrates (solution A) and aqueous sodium carbonate (solution B) as a precipitator to the reactor under vigorous stirring using a mechanical stirrer (IKA, cylindrical shape, 30 cm length) at about 550 rpm at 70 °C under air atmosphere. The pH was kept at 7.5± 0.3 during precipitation by controlling the flow rates of the solutions. After aging for 40 min at 70 °C, the precipitate was filtered and dried at 110 °C overnight under a static air condition. The final solid was then calcined in a tube furnace under flowing air condition at 380 °C for 6 h at a heating rate of 3 °C/min [2]. The structural form of the prepared sample (CO-PRE) is as CuO/ZnO/Al_2O_3.

4. Sol-gel Method

The CuO-SiO_2 nanocatalyst was prepared by the sol-gel technique from $Si(OC_2H_5)_4$ and $Cu(NO_3)_2\cdot3H_2O$ [13,14]. Ethanolic solutions of TEOS and $Cu(NO_3)_2.3H_2O$ were mixed in a container and heated to 50-55 °C when appropriate amounts of water (36 g) and oxalic acid (17.33 g) were added to the mixture. After 2 h stirring using a mechanical stirrer (IKA, cylindrical shape, 30 mm length), ethanol was removed from the clear sol and the sol was allowed to form a gel in air. The gel was dried in an oven by gradual increasing the temperature to 110 °C overnight under a static air condition. The sample was then powdered and calcined in a tube furnace under flowing air condition at 380 C for 6 h at a heating rate of 3 °C/min. The sample was named as SG.

5. Impregnation Method

The amorphous SiO_2 (274 m^2/g, total pore volume 0.96 cm^3/g, supplied by Sasol Company) was employed as the support and pretreated at 500 °C for 10 h in a muffle furnace under flowing air condition (impurity and access gas were removed from the active sites). After that, an aqueous solution of copper nitrate prepared at 65 °C temperature of water bath was added to the support vessel in the muffle furnace. Then, the furnace pressure was reduced to 500 mmHg by vacuum pump (the vacuum was reduced during the impregnation). The impregnation was continued for 6 hours. The resulting cake was dried at 110 °C overnight under a static air condition. The final solid was then calcined in a tube furnace under flowing air condition at 380 °C for 6 h at a heating rate of 3 °C/min and was named as IM [13].

6. Catalyst Characterization

The BET surface area (S_{BET}), total pore volume (V_P) and mean pore diameter (d_P) were measured by using the N_2 adsorption-desorption isotherm at normal boiling point of nitrogen (77 K) with

a NOVA 2200 instrument (Quantachrome, USA). Prior to the adsorption-desorption measurements, all the samples were degassed at 393 K under N_2 flow for 3 h to remove the moisture and other adsorbates.

The XRD patterns of all the calcined samples were recorded on a Bruker d_8 advance (40 kV, 30 mA) X-ray diffractometer using a Cu-K$_\alpha$ radiation source (λ=1.5406 Å) and a nickel filter in the 2θ range of 5° to 80°. The phases were determined by using Joint Committee on Powder Diffraction Standard (JCPDS) files.

The chemical compositions of nanocatalysts (Cu, Zn, Al, Si, Mg, Fe, P and Cl) were determined by an X-ray fluorescence (Phillips, Model PW2404) based on ASTM E 1621-05 standard. Also, the C content was measured by chemical analysis method (wet chemistry) based on ASTM E 1915-11 standard. Loss on ignition (L.O.I) measurement was carried out by treatment of samples at 750 °C for 1 h.

The bulk reduction behavior of the calcined samples was studied by a BELCAT-A system. 0.05 g of each sample (size 0.09-0.21 mm) was initially heated under helium flow (40 NmL/min) at a rate of 10 °C/min to 200 °C for 20 min and then was cooled to room temperature under the same flow. Then, the reducing gas (5% H_2 in Ar) was introduced at 50 NmL/min and the temperature was raised at a rate of 10 °C/min until it reached 700 °C. The effluent gas was passed through a cooling trap (at a temperature lower than −50 °C) to condense and collect the water generated during the reduction process. A thermal conductivity detector (TCD) was used to determine the amount of H_2 consumed. The K value of the TPR characteristic was 83.

The specific surface of metallic copper and copper dispersion both were measured by decomposition of N_2O using BELCAT-A system according to the following reaction:

$$2Cu(s)+N_2O \rightarrow Cu_2O(s)+N_2$$
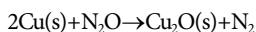
In each test, about 20 mg of nanocatalyst was reduced at 390 °C in 10% H_2/He for 30 min and then the temperature was cooled to 60 °C at ambient pressure under flow of helium. After that, a flow of pure N_2O was passed through the nanocatalyst bed for 30 min at 60 °C. Then, the inert gas (He) was switched on at 40 NmL/min for 30 min at the same temperature. Next, the reducing gas (10% H_2 in Ar) was introduced at 50 NmL/min and the temperature was raised at a rate of 5 °C/min until it reached 320 °C. The effluent gas was passed through a cooling trap (at a temperature lower than −50 °C) to condense and collect the water generated during the reduction process. A TCD was used to determine the amount of H_2 consumed.

The copper dispersion (D=Cu$_{surface\ atoms}$/Cu$_{total\ atoms}$) was calculated by assuming a stoichiometry of N_2O : Cu=0.5 from surface metallic copper sites to form Cu_2O. In this work, a surface copper density of 1.46×10^{19} atoms/m^2 was used for the copper metal area calculations [20,21].

The nature of the carbonaceous compounds (aliphatic or aromatic) deposited on the spent catalysts was determined by FT-IR method using an 8400S Laboratories FT-IR spectrometer (Shimadzu, Japan) equipped with a MCT-NB cryogenic mercury detector with 2 cm^{-1} resolution. The FT-IR transmittance and absorbance spectra were recorded in 4,000-500 cm^{-1} region. Potassium bromide (KBr)

powder was used as the sample matrix and reference material. For the FT-IR measurements, a mixture of powdered material (KBr and nanocatalyst) was pelleted in a self-supporting disc, 25-30 mg cm^{-2} and 0.1-0.2 mm thick, which was placed in an FT-IR cell and then measurements were carried out at room temperature.

Field-emission scanning electron microscopy (JEOL JSM-5600LV FE-SEM) with an acceleration voltage of 15 kV and transmission electron microscopy (Zeiss EM-900 TEM) with an acceleration voltage of 50 kV and 80 kV were used to investigate size and morphology of the nanocatalysts. The catalysts were dispersed in ethanol by ultrasonication, then one drop of each resulting suspension was poured on the FE-SEM sample holder and TEM sample grid until it was dried to use for the FE-SEM and TEM observations. The samples were coated with gold before the FE-SEM analysis.

7. Catalytic Performance Tests

Vapor-phase dehydrogenation of 2-butanol was carried out in the Chemical Data Systems (CDS) unit. Fig. 1 demonstrates a simplified flow diagram of the CDS unit. The reactor system was entirely placed in a temperature-controlled three-zone furnace, so that the feed could be preheated and the products could be sent directly to the gas chromatograph analyzer without condensation. To avoid any product condensation, the transfer line from reactor outlet to the separator vessel was externally heated and maintained at 120 °C. The reactor was a fixed-bed reactor (stainlessness steel, i.d. 12.7 mm and length of 305 mm). In a typical run, 3 g of nanocatalyst (size 16-25 mesh or 0.19-0.71 mm) was loaded in the middle section
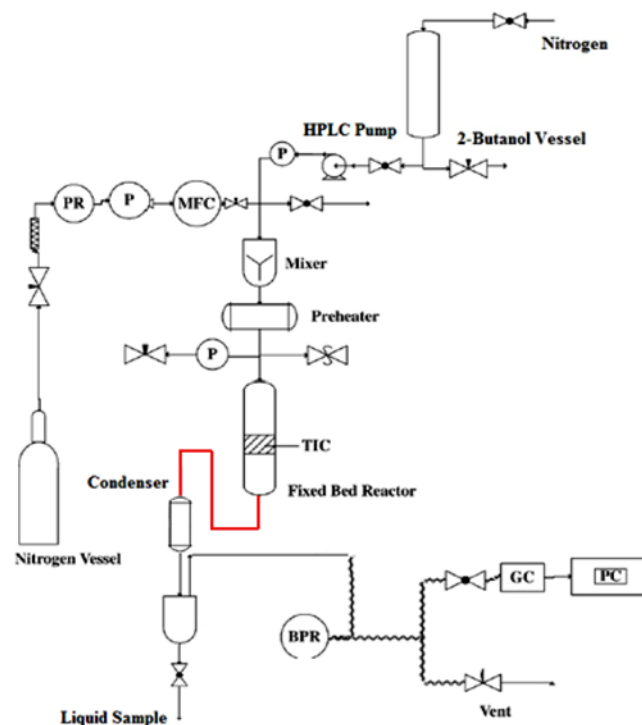

Fig. 1. A simplified flow diagram of the chemical data systems (CDS) unit.

MFC. Mass flow controller   PR. Pressure regulator
BPR. Back pressure regulator   TIC. Temperature regulator
PC. Pressure computer
Red line. Heating line with electrical heat trace system

of the reactor tube and 2-butanol was pumped by a WellChrom HPLC K-120 pump with liquid hourly space velocity (LHSV) of 4 mL/(h·g$_{cat}$). Prior to the catalytic activity measurements, the samples were reduced in situ at a heating rate of 1 °C/min under the flow of a mixture of H$_2$ (10 mL/min) and N$_2$ (75 mL/min) at 265 °C for 15 h under atmospheric pressure. After that, the flow of the reducing gas was stopped and then 2-butanol was pumped from a feed tank to pre-heater and activity tests were conducted at 260 °C and atmospheric pressure for 150 h. The reactor outlet was sent to the condenser for collecting the liquescent components. A high-pressure condensation trap was placed in series to ensure complete trapping of the liquid products. The gaseous products were analyzed by an on-line gas chromatograph (GC) of Varian CP-3800 equipped with a TCD and FID detectors in which a PoraPlot-Q-HT column was used to separate the reaction main by-products (CO and C$_4$ cut). Liquid samples were analyzed with a Varian CP-3800 gas chromatograph equipped with a TCD detector in which a CP-Wax-52CB column was used to separate the reaction products (MEK, SBA, H$_2$O, Butanone, C$_8$H$_{14}$O, and C$_8$H$_{18}$O).

As measures of the catalytic performance and for the purpose of quantitative comparison with commercial catalysts, the SBA conversion (X$_{SBA}$, %), yield of MEK (Y$_{MEK}$, %) and selectivity to MEK (S$_{MEK}$, %) were used. These were defined as follows:

$$X_{SBA} = \frac{(Mole_{C_4H_9OH})_{inlet} - (Mole_{C_4H_9OH})_{outlet}}{(Mole_{C_4H_9OH})_{inlet}} \times 100$$

$$S_{MEK} = \frac{(Mole_{MEK})}{(Mole_{MEK} + Mole_{byproduct})} \times 100$$

$$Y_{MEK} = (S_{MEK} \times X_{SBA}) \times 100$$

For the determination of the optimum operating conditions, S$_{MEK}$ was selected as the main response. Also, for preparation conditions screening purposes and comparison of activities, the results were compared on the basis of total catalyst mass.

RESULTS AND DISCUSSION

1. Characterization Results

The textural properties of the nanocatalysts are listed in Table 1. The total surface area and pore volume of the catalyst prepared by impregnation using SiO$_2$ support (Sample IM) is the highest (208.9 m^2/g), while the nanocatalyst prepared by the co-precipitation method (COPRE sample) had the lowest surface area (69.4 m^2/g). The IM sample exhibited a clear decrease in specific surface area and total pore volume compared to the support (274.1 m^2/g). This is expected because the pores of the support are partially filled by CuO parti-

Table 1. Textural properties of the different samples

Sample	Surface area (m^{2}g^{-1})	Total pore volume (cm^{3}g^{-1})	Crystallite size (nm)[a]
COPRE	69.4	0.42	23.8
SG	94.1	0.21	21.9
SiO$_2$ support	274.1	0.98	-
IM	208.9	0.83	25

[a]Determined from the XRD results
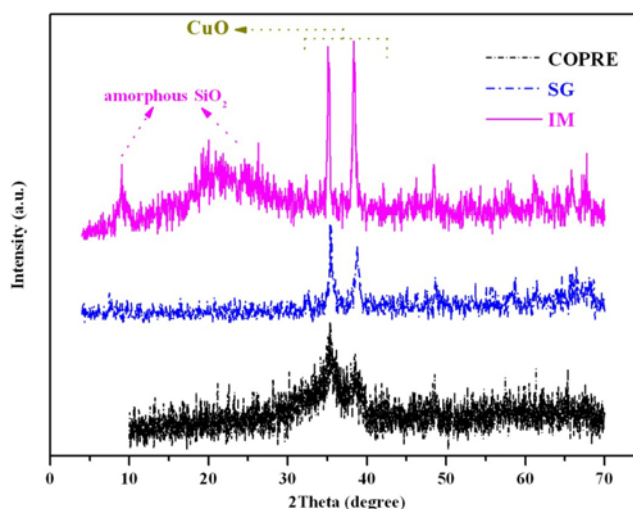
Fig. 2. The XRD patterns of the prepared nanocatalysts: (a) COPRE, (b) SG and (c) IM.

cles. In addition, using oxalic acid as the precipitating agent (SG sample), the complex is decomposed into carbon dioxide, water and probably other components during calcination. The produced gasses prevent agglomeration and help to create pores and fine particles with high surface areas in the final products. As a result, the influence of support on the surface area is more dominant compared to the effect of preparation method.

The XRD patterns of the samples showed the signal of copper oxide (CuO) phase in all of nanocatalysts (Fig. 2). The intensities of the peaks were slightly lower in SG, and especially in COPRE sample, while IM sample made by wet-impregnation had the highest peak intensities, and consequently, the largest crystallite size. Moreover, the COPRE and SG nanocatalysts exhibited additional peaks which correspond to crystalline phases of ZnO, ZnAl$_2$O$_4$, CuAl$_2$O$_4$ and SiO$_2$. However, the IM nanocatalyst did not show the silicon dioxide signals, implying the SiO$_2$ particles were amorphous.

According to the XRD results, the mean crystalline sizes (d) of CuO nanoparticles were estimated using Scherer's equation (d= 0.9 λ/b cosq) [22] where λ=1.54 Å is the wavelength of the X-ray radiation used, θ is the Bragg diffraction angle of the XRD peak and β is the measured broadening of the diffraction line peak at an angle of 2θ and is the full width diffraction peak at half maximum intensity (FWHM).

Table 1 also presents the calculated crystallite sizes of CuO in the samples. The crystallite sizes were decreased in the order: IM> COPRE>SG. The results illustrated that the nanocatalyst prepared by the addition of oxalic acid as precipitator had the smallest average crystallite size. Therefore, it can be concluded that the oxalic acid was templated and especially affected the textural properties and led to a sample with the smallest crystallite size.

The chemical compositions of the different nanocatalysts used in the present study are given in Table 2. In all cases, the empirical values of the catalyst compositions based on XRF analysis were in good agreement with the nominal values.

The TPR profiles (Fig. 3) showed that all of the prepared nanocatalysts have a main reduction peak, which can be attributed to

Table 2. Compositions and chemical properties of the different samples

Sample	Chemical components (%)						
	CuO	ZnO	Al$_2$O$_3$	SiO$_2$	MgO	Carbon (C)	L.O.I
CCS	32.3	-	-	49.6	10.1	1.6	4.66
CCFRI	44.2	40.7	4.6	-	0.34	1.75	9.13
COPRE	43.7	34.7	5.6	1.3	0.41	2.5	13.82
SG	23.9	-	-	73.6	0.16	1.4	-
IM	18.1	-	-	75.7	-	1.9	5.91

L.O.I. is "Loss of Ignition"
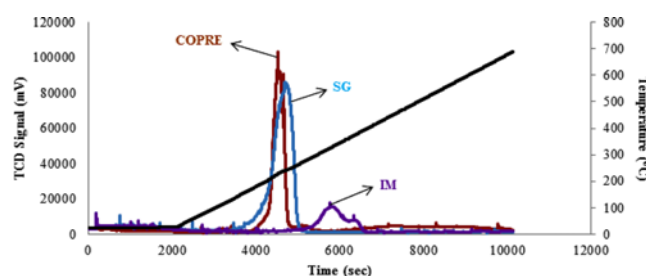
Fig. 3. The TPR profiles of calcined nanocatalysts.

the reduction of CuO species to metallic copper (Cu^0). The reduction peak temperature varies from 222 to 327 °C, in which the COPRE sample exhibiting the highest catalytic activity had the lowest reduction peak temperature and the highest percent of CuO reduction. Table 3 shows the reduction peak temperature and the percentage of reduction for nanocatalysts that have been prepared by different methods. It appears that 265 °C was a suitable reduction temperature and it was used for all nanocatalysts. Moreover, TPR profile of COPRE sample demonstrated a broad peak at 300-600 °C temperature range, which could be attributed to the reduction of copper oxide species in form of copper aluminate (CuAl$_2$O$_4$) that was formed during calcination by solid-state reaction of CuO with the Al$_2$O$_3$ species. Moreover, the XRD pattern of COPRE sample confirmed the presence of this crystalline phase.

The specific copper surface area and the amount of exposed copper (Cu^0) for the fresh nanocatalysts determined by N$_2$O titration are given in Table 4. One observes that these values for COPRE nanocatalyst are the highest, while SG and IM samples display values that are about 25% and 85% lower for the exposed copper and

Table 4. The N$_2$O-titration data for different copper nanocatalysts

Sample	Exposed copper (μmol Cu/g$_{cat}$)	Specific copper surface area (m^2/g cat)	Cu-dispersion[a] (%)
COPRE	1224	50.49	15.85
SG	910	37.54	6.39
IM	192	7.92	5.97

[a]Copper dispersion=exposed copper atoms/total copper atoms

specific copper surface area, respectively. It implies that both Zn and Al can increase the copper surface area and the amount of exposed copper. Furthermore, it indicates that both of them are structural promoters that act as spacers that prevent copper oxide from sintering [23,24]. When these two promoters are used together, this effect is more pronounced.

The copper dispersion, defined as the ratio of exposed copper to the total amount of copper atoms, is also included in Table 4. The presence of Zn and Al in the structure of COPRE nanocatalyst can also increase the dispersion of Cu nanoparticles on the surface. The lowest value belongs to the IM sample.

Figs. 4 and 5 represent the FE-SEM and TEM images of the nanocatalysts after calcination, respectively. According to the FE-SEM images, the preparation procedure influences the morphology and particle size of copper-based nanocatalysts. The as-synthesized samples consist of differently shaped particles. COPRE sample (Fig. 4(a)) had irregular morphology and the other samples (Figs. 4(b) and 4(c)) look as regular rod or planar rod shape morphologies with different sizes. Also, the FE-SEM image of COPRE sample showed strong agglomeration of particles, resulting in no distinctive crystal shape. The FE-SEM study confirms that the morphology of the final product is dependent on the preparation procedure used during synthesis. Moreover, the TEM images exhibited morphology and particle size of these nanocatalysts. All of the nanocatalysts exhibited particle sizes in the range of 5-20 nm. It can be concluded that the nanocatalysts with smaller particle sizes should have better performance owing to increasing the number of active sites.

2. Performance and Screening Test Results

The catalytic activity for vapor phase 2-butanol dehydrogenation on COPRE, SG and IM nanocatalysts at steady state is presented in Table 3. The highest selectivity to MEK (main product of the dehydrogenation process) and the highest 2-butanol conversion were obtained for COPRE nanocatalyst. For the IM sample,

Table 3. The TPR data and catalytic activities of 2-butanol dehydrogenation on different copper nanocatalysts

Sample	TPR data		Catalytic performance[a]		
	T$_{red.}$ (°C)[b]	Percent of reduction (%)[c]	SBA conversion (%)	MEK selectivity (%)	Yield (%)
COPRE	222	98.8	93.1	90.3	84.1
SG	243	80.1	92.2	89.01	82.1
IM	327	72.4	77.2	44.1	33.2

[a]Reaction conditions: T=260 °C, P=atmospheric pressure, LHSV=4 mL/(h·g$_{cat}$), Time of stream (TOS)=150 h, no carrier gas; nanocatalysts: 3.0 g
[b]T$_{red}$: Temperature of reduction maxima
[c]Degree of reduction=hydrogen consumption from TPR/hydrogen consumption from stoichiometry equation
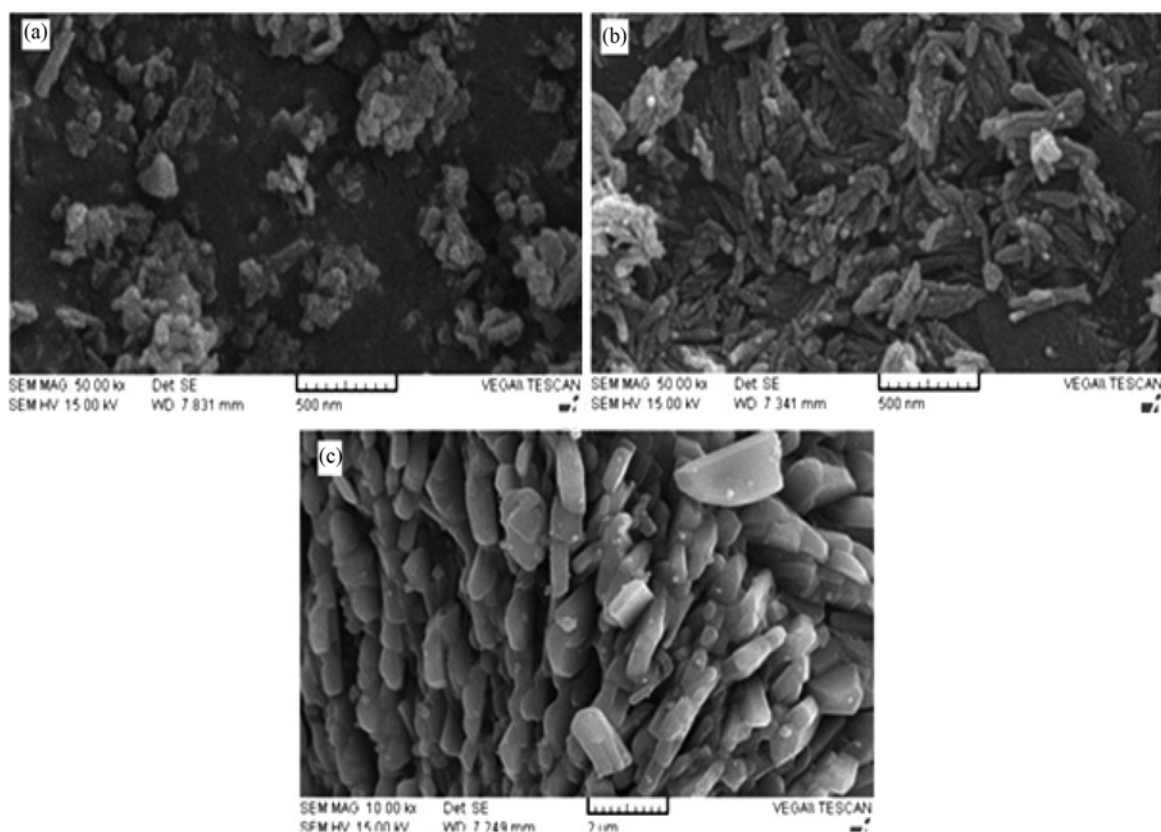
Fig. 4. The FE-SEM images of the different calcined nanocatalysts: (a) CO-PRE, (b) SG and (c) IM nanocatalysts.
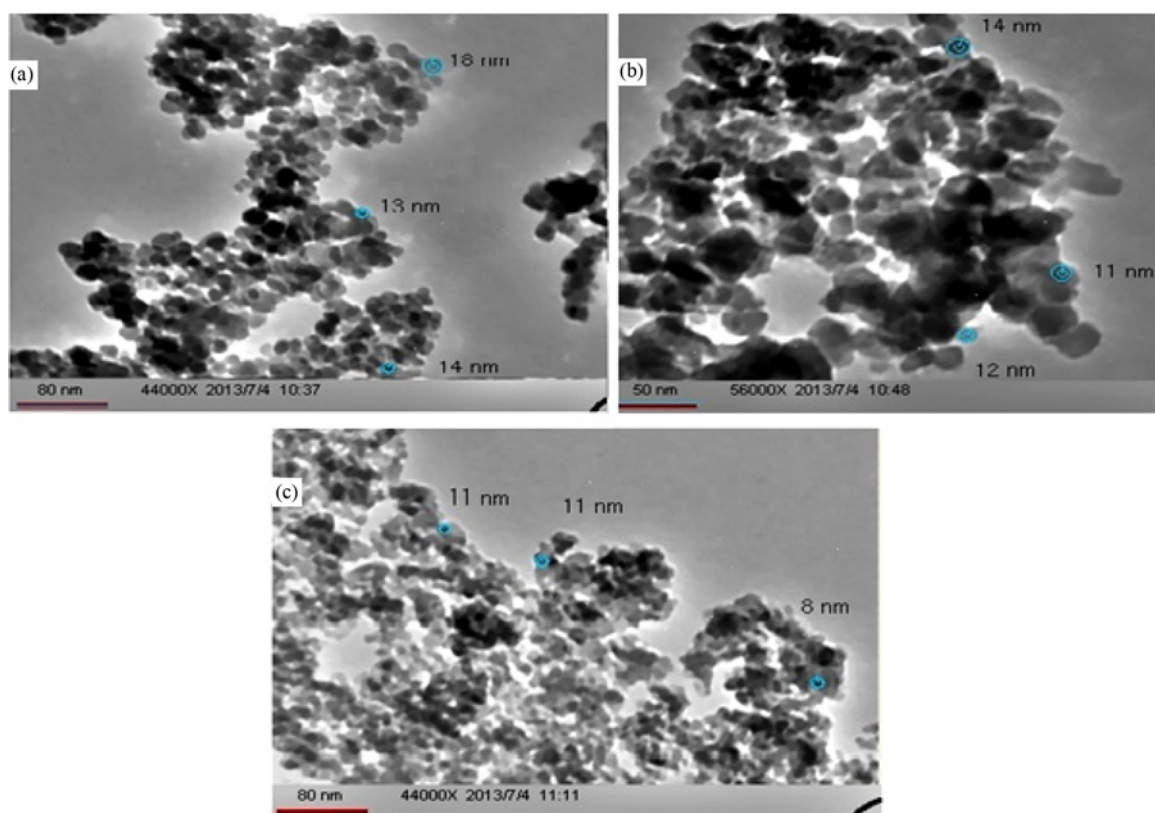

Fig. 5. The TEM images of CuO nanoparticles of the (a) COPRE, (b) SG and (c) IM calcined nanocatalysts.
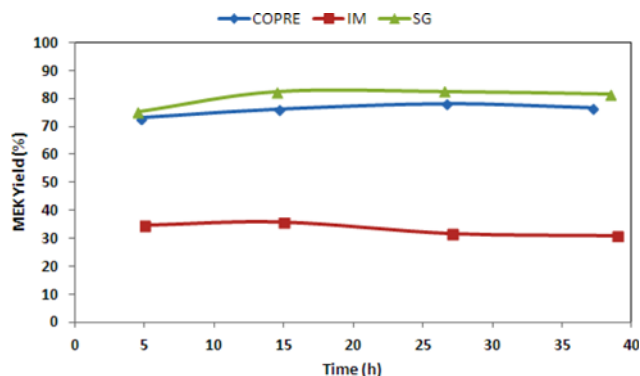
Fig. 6. Yield of the reaction products over the different catalysts calcined as a function of time.

Fig. 7. The FT-IR spectra of the prepared nanocatalysts: (a) COPRE, (b) SG and (c) IM.

very low selectivity to MEK (44.1%) and low conversion of 2-butanol (77.2%) were observed. The N_2O titration result implies that the dispersion of copper species in the COPRE nanocatalyst was better than that in the SG and IM samples. The TPR results confirm that the degree of reduction of the copper oxide particles to metallic copper (Cu^0) as an active site for dehydrogenation of 2-butanol and temperature of reduction maxima is very suitable in the COPRE nanocatalyst. As a result, the conversion of 2-butanol and selectivity to MEK on the COPRE nanocatalysts both were higher than those on the IM nanocatalyst. According to Table 3, very low catalytic activity was observed for the IM sample, but the catalytic activity of the SG sample was close to that of the COPRE sample. Samples SG and COPRE could also be compared based on the starting materials. The SG sample was synthesized from high cost materials, such as ethanolic solutions of TEOS and copper nitrate, whereas in synthesis of COPRE sample, inorganic and inexpensive precursors such as copper hydroxide carbonate, zinc oxide, aluminum nitrate nonahydrate and nitric acid were employed. The COPRE nanocatalyst is superior to the SG sample from the economical point of view.

Fig. 6 depicts the reaction yield over the calcined nanocatalysts with the time-on-stream at 533 K. The yield of 2-butanol was fairly constant with the time-on-stream over the different nanocatalysts. The yield of MEK was lower over the IM nanocatalyst. The main by-products were carbon monoxide, C_4 olefins with smaller amounts of C_8 oxygenates. The latter products are formed through dehydration and oligomerization reactions catalyzed by acid sites. Regarding the dehydration of alcohol, it is well known that dehydration is related to the acidic sites on the nanocatalyst surface. In this work, we did not introduce the acidic sites to the nanocatalysts surface during the preparation. For the IM nanocatalyst, the high by-products may be due to the high H^+ existing on the SiO_2 surface, while for the COPRE and SG nanocatalysts, Cu^0 is the only active copper species on the nanocatalyst surface during the reaction; thus there was little by-product. Consequently, to obtain high conversion of 2-butanol and high selectivity to MEK, preparing high dispersion Cu^0 nanocatalyst is necessary.

FT-IR spectroscopy was used to acquire information about the nature of the carbonaceous compounds deposited on the used catalysts. Fig. 7 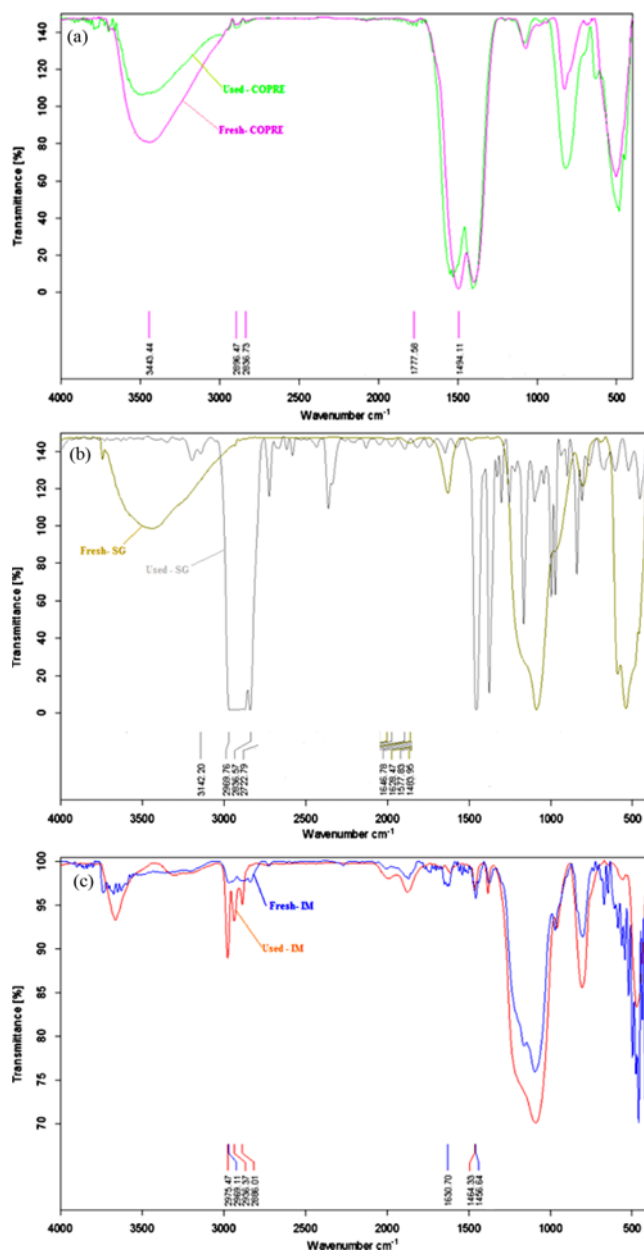demonstrates the FT-IR vibrational spectra of the coke deposited on the deactivated nanocatalysts with similar feed composition. The peaks in the spectral range of 2,800-3,000 cm^{-1} correspond to the vibrations of C-H bonds of paraffins, olefins (asymmetric and symmetric stretching) and single-ring aromatics [25]. FT-IR absorbance spectra of different samples showed that the intensities of the bands corresponding to aliphatics and single-ring aromatics coke deposited on surfaces of deactivated SG (Fig. 7(b)) and IM (Fig. 7(c)) nanocatalysts were higher than those of COPRE sample (Fig. 7(a)). The FT-IR spectra of COPRE nanocatalyst indicated a negligible amount of aliphatic carbonaceous compounds on the deactivated nanocatalyst surface. The intensities of the bands corresponding to conjugated double bonds at 1,500-1,600 cm^{-1} are almost similar for all samples [26]. Studying the nature and quan-

tity of the coke deposited on the deactivated catalyst surface can be useful in the catalyst screening stage. It is clear that the samples with low coke and more aliphatic type of carbonaceous compounds are more desirable, because the deposited coke can easily be eliminated from the nanocatalyst surface by appropriate oxidative treatments. In this case, the nanocatalyst has a better regenerability.

3. Optimization by Response Surface Method

3-1. Optimization Method

Following a preliminary screening of the nanocatalysts based on preparation method, the response surface method (RSM) was used for the design of experiments and analyzing the results for the selected nanocatalyst type. The objective of RSM is to optimize the response based on the factors investigated [27-31]. In this work, the developed response surface design was based on central composite design (CCD) and accordingly, a quadratic regression model was considered for developing the response surface models of second order as indicated in Eq. (1) where R denotes the predicted response of the process, x_i refers to the coded factors and b_0, b_i, b_{ii}, b_{ij} are the regression coefficients.

$$R = b_0 + \sum_{i=1}^{n} b_i x_i + \sum_{i=1}^{n} b_{ii} x_i^2 + \sum_{i<j}^{n} b_{ij} x_i x_j \qquad (1)$$

After performing the experimental test runs and determining the coefficients of the model, insignificant coefficients for terms which did not influence the response variation were removed from the fitted model. Reducing the model in this way simplified the regression model while maintaining its high accuracy. The P-value being calculated for all of the coefficients is a suitable criterion for determining which coefficient is statistically insignificant and should be removed from the model. The adequacy of the model is determined by performing the Fisher test, which results in calculation of the F-value. Analysis of variance (ANOVA) table gives two F-values including the regression related F-value and the lack-of-fit related F-value. The fitted model will be adequate if the regression related F-value is greater than the related F_{tab} and the lack-of-fit related F-value is less than the related F_{tab}. The degree of freedom (DF) for the regression and residual error sources directs one to determine the related F_{tab} using the F-distribution table. In this manner, the lack-of-fit related F_{tab} is determined using degree of freedom (DF) for the lack-of-fit and pure error sources [27-31]. Note that the residuals will be distributed normally if the model provides an adequate goodness-of-fit. If the P-value for the Anderson-Darling test is greater than the chosen significance level (usually 0.05), it can be concluded that the residuals follow a normal distribution [14,27]. This work attempted to apply the central composite design (CCD) method as a division of the response surface method (RSM) to design the experiments and analyze the empirical results with the aim of maximizing S_{MEK} and X_{SBA} as the response parameters.

3-2. Experimental Design

The screening results of the previous section confirmed that the $CuO/ZnO/Al_2O_3$ nanocatalyst prepared by co-precipitation exhibited the best performance. Because of the complex nature of co-precipitation systems incorporating several variables, often interacting, precise modeling of the system could be very complicated or impossible. In contrast, empirical models with statistical technique analyses such as response surface method (RSM) appear to

Table 5. Factors and their levels in the CCD method

Factor	Low level	High level
$T_{(pre)}$	65	75
$T_{(Age)}$	65	80
$pH_{(pre)}$	6.3	7.6
Cu/Zn molar ratio	1	2.5

be quite useful.

The optimization of the main and most effective parameters during preparation was investigated by a central composite design (CCD) with four preparation factors (precipitation temperature (T_{Pre}), aging temperature (T_{Age}), pH of precipitation stage and Cu/Zn molar ratio) in five levels that were selected as the fixed factors. The low and high levels of the factors were chosen based on information from the literature and our previous results of bi-functional nanocatalysts [32,33]. The preparation parameters kept constant during all nanocatalyst preparation runs were as follows: stirring blade=impeller; impeller speed=550 rpm; concentration of solutions=1 M and addition rate of solutions=5 mL/min. To create a response surface design, the type of design, number of independent variables or factors, name of factors, their upper and lower levels (Table 5), value of response and replication points should be entered into the software. The experimental plan was generated using the Design Expert 7.0.0 software involving 24 runs and 3 replicates of the central point. Therefore, totally, the software suggested 27 nanocatalyst preparation test runs which are presented in Table 6. Table 6 also reports the time-average experimental SBA conversions, MEK selectivities and yields obtained within 50 hours-on-stream.

CCD allows for the simultaneous study of the effects that several factors may have on a process. As given in Table 6, five levels of precipitation temperature (65, 67.5, 70, 72.5, 75 °C), aging temperature (65, 68.75, 72.5, 76.25, 80 °C), pH of precipitation stage (6.3, 6.62, 6.95, 7.27, 7.6) and Cu/Zn molar ratio (1, 1.38, 1.75, 2.13, 2.5) were investigated as varying factors. Based on the residual results, among 27 designed experiments, the output data of four runs, that is, runs 5, 16, 13 and 27, were identified as outliers. Therefore, appropriate modeling of experimental design was performed based on the remaining 23 runs.

By reducing Eq. (1), the final equation was obtained for the response including MEK selectivity (R) in terms of coded variables using modified quadratic model (Eq. (2)) with adequate goodness-of-fit. Note that x_1, x_2, x_3 and x_4 represent the experimental factors i.e. pH, Cu/Zn molar ratio, T_{Pre} and T_{Age}, respectively.

$$R = 81.73 + 1.64x_1 - 1.89x_2 + 0.94x_3 + 0.88x_3^2 + 0.99x_2^2 \qquad (2)$$
$$+ 1.66x_1x_2 - 2.02x_1x_3 + 1.59x_3x_2$$

After the experimental data based on the CCD method (Table 6) were collected, the general quadratic model for the fixed four-factor effects was used to conduct an analysis of variance (ANOVA) to determine which factors would affect the catalytic activity (especially MEK selectivity, S_{MEK}) more significantly. Various statistical data (standard error of estimate, sum of squares of the errors, F statistics, and P value) were examined. The ANOVA computes

Table 6. Specifications of designed experiments by the CCD method

Run no.	Factors and levels				Responses		
	$T_{(pre)}$	$pH_{(pre)}$	$T_{(Age)}$	Cu/Zn molar ratio	X_{SBA} (%)	S_{MEK} (%)	Y_{MEK} (%)
Cu/Zn/Al-1	67.5	7.27	68.75	1.38	94.34	88.72	83.71
Cu/Zn/Al-2	72.5	6.62	76.25	2.13	92.25	85.99	79.31
Cu/Zn/Al-3	72.5	7.27	68.75	2.13	91.36	87.21	79.67
Cu/Zn/Al-4	70.0	6.95	72.50	1.75	93.79	82.85	77.69
Cu/Zn/Al-5	72.5	7.27	68.75	1.38	95.08	79.33	75.39
Cu/Zn/Al-6	70.0	6.95	72.50	2.50	93.52	82.10	76.79
Cu/Zn/Al-7	72.5	7.27	76.25	2.13	92.89	84.08	78.11
Cu/Zn/Al-8	67.5	7.27	76.25	1.38	92.89	87.44	81.23
Cu/Zn/Al-9	72.5	6.62	68.75	1.38	92.24	86.08	79.43
Cu/Zn/Al-10	70.0	7.60	72.50	1.75	93.12	85.73	79.83
Cu/Zn/Al-11	75.0	6.95	72.50	1.75	90.66	86.80	78.71
Cu/Zn/Al-12	67.5	6.62	76.25	1.38	92.94	80.89	75.19
Cu/Zn/Al-13	67.5	6.62	76.25	2.13	91.53	85.34	78.12
Cu/Zn/Al-14	67.5	7.27	68.75	2.13	92.89	83.63	77.72
Cu/Zn/Al-15	70.0	6.30	72.50	1.75	93.78	78.77	73.87
Cu/Zn/Al-16	67.5	6.62	68.75	2.13	93.49	80.03	74.81
Cu/Zn/Al-17	72.5	7.27	76.25	1.38	94.01	82.63	77.66
Cu/Zn/Al-18	67.5	7.27	76.25	2.13	92.60	84.72	78.45
Cu/Zn/Al-19	70.0	6.95	80.00	1.75	93.45	80.62	75.34
Cu/Zn/Al-20	72.5	6.62	76.25	1.38	92.76	88.15	81.77
Cu/Zn/Al-21	70.0	6.95	65.00	1.75	92.43	82.39	76.16
Cu/Zn/Al-22	67.5	6.62	68.75	1.38	93.14	83.89	78.12
Cu/Zn/Al-23	72.5	6.62	68.75	2.13	93.49	79.87	74.67
Cu/Zn/Al-24	65.0	6.95	72.50	1.75	91.65	83.85	76.88
Cu/Zn/Al-25	70.0	6.95	72.50	1.75	94.23	81.79	77.07
Cu/Zn/Al-26	70.0	6.95	72.50	1.75	92.33	80.28	74.15
Cu/Zn/Al-27	70.0	6.95	72.50	1.00	93.89	78.45	73.66

such quantities as the degrees of freedom (DF), F-value and P-value (P). An important statistical parameter in ANOVA table is the P-

Table 7. The ANOVA analysis results for S_{MEK} based on regression models for tests (modified quadratic model)

Source	DF	Seq SS	F	P	R-squared	Adj R-squared
Model	8	131.88	6.86	0.0010	0.7966	0.6804
pH	1	50.07	20.82	0.0004		
Cu/Zn	1	46.57	19.37	0.0006		
$T_{Pre.}$	1	16.5	6.86	0.0202		
pH×Cu/Zn	1	25.63	10.66	0.0056		
pH×$T_{Pre.}$	1	37.86	15.75	0.0014		
Cu/Zn×$T_{Pre.}$	1	23.55	9.79	0.0074		
Cu/Zn×Cu/Zn	1	13.66	5.68	0.0319		
$T_{Pre.}$×$T_{Pre.}$	1	19.58	8.14	0.0128		
Residual	14	33.66				
Lack of fit	12	30.34				
Pure Error	2	3.33				
Total	22	165.54				

value. The P-value for a term tells whether the effect for that term is significant or not: if P is less than or equal to the α-level selected, then the effect for the term is significant (the α-level was 0.05). Since the P-values for T_{Age} and interaction of T_{Age}×pH were all >0.05, the effect of the above-mentioned terms were insignificant and should be removed from the model. The results of ANOVA analysis on modified quadratic model for the selectivity to MEK are given in Table 7, indicating all factors and their interactions have P-values less than 0.05, which means that the effects of these factors as well as two- and three-factor interaction effects on the selectivity as the response parameters are significant. From Table 7 the F-values of all factors for these conditions are considerably greater than the extracted F-value of tables with 95% confidence. This means that the variances of all factors are significant compared with the variance of error and all of them have important effects on the response [21].

4. Analysis of Modeling and Evaluation of Accuracy/Validity

In a selectivity regression model, there are ten significant coefficients because their P-values are less than 0.05. The significance of a coefficient depends on the amount of P-value. The smaller the P-value, the more significant is the corresponding coefficient. According to the P-values, the effects of pH and Cu/Zn molar ratio on the
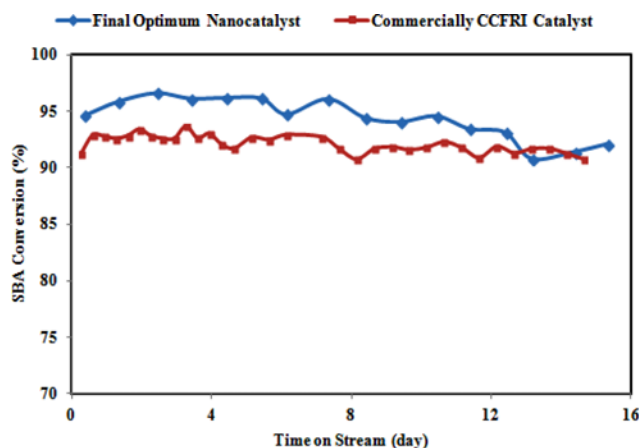
Fig. 8. Long term SBA conversion versus time-on-stream (T=260 $^{\circ}$C, P=1.2 bar, LHSV=4 mL/(h·g$_{cat}$)).

response were more significant than those of other factors (Table 7). The coefficients with the P-values >0.05 should be retained in the fitted model because of reduction in the adjusted R value after removing them. The suggested model for the selectivity variations was adequate because not only F-value for the regression model was greater than F_{tab} with the P-value <0.05 but also F-value for the lack-of-fit was less than F_{tab} with P-value >0.05 (Table 7).

5. Selection of Optimum Operating Conditions for the Catalyst Preparation

Finally, after analysis of modeling and evaluation of a suitable model, the optimum operating conditions were selected based on Eq. (2) for the nanocatalyst preparation. For this purpose, numerical optimization was used and the target for each response and their minimum and maximum values were entered into the software. The maximum point in each graph marks the optimum value of a particular factor. Therefore, according to the numerical optimization and maximum points, the factor levels indicating the optimum conditions were as follows: $T_{Pre.}$=67.5 $^{\circ}$C, $T_{Age.}$=68.75 $^{\circ}$C, pH=7.27 and Cu/Zn molar ratio=1.38.

The XRF result confirmed that the structural formula of the final optimum nanocatalyst was similar to the CCFRI as the commercially available catalyst. Fig. 8 presents a parity plot of the long-term stability for the CCFRI sample and the final nanocatalyst which was prepared under the optimum conditions. As can be seen, this nanocatalyst indicates an excellent stability for this reaction.

CONCLUSIONS

Copper-based nanocatalysts with the general formula of CuO/ZnO/Al$_2$O$_3$ and CuO/SiO$_2$ were prepared by different methods (co-precipitation, sol-gel and impregnation) and characterized by a variety of physicochemical, structural, spectroscopy, microscopy, and catalytic measurements for the 2-butanol dehydrogenation reaction. The activity and MEK selectivity of the nanocatalysts increased in the following sequence:

CuO/ZnO/Al$_2$O$_3$ (co-precipitation)>CuO/SiO$_2$ (sol-gel)
   >CuO/SiO$_2$ (impregnation)
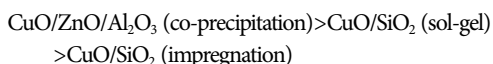
In the second section, the effects of some operating conditions in the precipitation method (precipitation temperature, aging temperature, pH of precipitation stage and Cu/Zn molar ratio) on the structure, physicochemical properties and catalytic performance (especially MEK selectivity) of CuO/ZnO/Al$_2$O$_3$ nanocatalysts were investigated and optimized. These experiments were designed according to central composite design (CCD) method with four factors in five levels and by performing twenty seven nanocatalyst preparation test runs. Under our experimental conditions, the main results can be summarized as follows:

- The precipitation temperature and pH of precipitation stage were the most important variables in this system, exerting strong influences on all analyzed process responses.

- There is a good agreement between predicted and experimental nanocatalyst activity such as MEK selectivity and SBA conversion.

- According to the statistical results, the optimum level of parameters that can maximize MEK selectivity are precipitation temperature=67.5 $^{\circ}$C, aging temperature=68.75 $^{\circ}$C, pH of precipitation stage =7.27 and Cu/Zn molar ratio=1.38. These results are valid at the experimental operational conditions ranges ($T_{Pre.}$=65-75 $^{\circ}$C, $T_{Age.}$= 65-80 $^{\circ}$C, pH=6.3-7.6 and Cu/Zn molar ratio=1-2.5).

REFERENCES

1. F. H. A. Bolder, *Ind. Eng. Chem. Res.*, **47**, 7496 (2008).
2. L. Zhenhua, H. Wenzhou, Q. Haoand and M. A. Kai, *Chinese J. Chem. Eng.*, **14**, 676 (2006).
3. J. N. Keuler, L. Lorenzen and S. Miachon, *Appl. Catal. A: Gen.*, **218**, 171 (2001).
4. D. Fang, W. Ren, Z. Liu, X. F. Xu, L. Xu, H. Lü, W. Liao and H. Zhang, *J. Nat. Gas Chem.*, **18**, 179 (2009).
5. O. W. Perez-Lopez, A. C. Farias, N. R. Marcilio and J. M. C. Bueno, *Mater. Res. B*, **40**, 2089 (2005).
6. G. S. Grover and R. V. Chaudhari, *J. Mol. Catal.*, **49**, 143 (1989).
7. N. Cheikhi, M. Kacimi, M. Rouimi, M. Ziyad, L. F. Liotta, G. Pantaleo and G. Deganello, *J. Catal.*, **232**, 257 (2005).
8. P. Driver, G. Glowa and J. C. Wren, *Radiat. Phys. Chem.*, **57**, 37 (2000).
9. J. F. Smetana, J. L. Falconer and R. D. Noble, *J. Membr. Sci.*, **114**, 127 (1996).
10. W. Zhu, L. Wang, Sh. Liu and Z. Wang, *React. Kinet. Catal. Lett.*, **93**, 93 (2008).
11. G. S. Jeon and J. S. Chung, *Korean J. Chem. Eng.*, **14**, 49 (1997).
12. Z. Wang, H. Ma, W. Zhu and G. Wang, *React. Kinet. Catal. Lett.*, **76**, 271 (2002).
13. Z. Wang, Q. Liu, J. Yu, T. Wu and G. Wang, *Appl. Catal. A: Gen.*, **239**, 87 (2003).

14. S. Lambert, C. Cellier, F. Ferauche, E. M. Gaigneaux and B. Heinrichs, *Catal. Commun.*, **8**, 2032 (2007).

15. Y. Han, J. Shen and Y. Chen, *Appl. Catal. A: Gen.*, **205**, 79 (2001).

16. H. F. Chang and Ch.-F. Yang, *Ind. Eng. Chem. Res.*, **36**, 2080 (1997).

17. M. Mapa, K. Sivaranjani, D. S. Bhange, B. Saha, P. Chakraborty, A. K. Viswanath and Ch. S. Gopinath, *Chem. Mater.*, **22**, 565 (2010).

18. E. M. Gaigneaux, S. R. G. Carrazan, P. Ruiz and B. Delmon, *Thermochim. Acta*, **388**, 27 (2002).

19. M. Khachani, M. Kacimi, A. Ensuque, J.-Y. Piquemal, C. C. Franc, O. Bozon-Verduraz and M. Ziyad, *Appl. Catal. A: Gen.*, **388**, 113 (2010).

20. G. R. Moradi, S Nosrati and F. Yaripour, *Catal. Commun.*, **8**, 598 (2007).

21. J. R. Jensen, T. Johannessen and H. Livbjerg, *Appl. Catal. A: Gen.*, **266**, 117 (2004).

22. D. Raoufi, *Renew. Energy*, **50**, 932 (2013).

23. M. S. Spencer, *Catal. Lett.*, **50**, 37 (1998).

24. K. C. Waugh, *Catal. Lett.*, **58**, 163 (1999).

25. F. Bauer and H. G. Karge, *Mol. Sieves*, **5**, 249 (2007).

26. B. Valle, P. Castano, M. Olazar, J. Bilbao and A. G. Gayubo, *J. Catal.*, **285**, 304 (2012).

27. M. S. Phadke and K. Dehnad, *Qual. Reli. Eng. Int.*, **4**, 105 (2007).

28. X. Han, Y. He, H. Zhao and D. Wang, *Korean J. Chem. Eng.*, **31**, 1810 (2014).

29. N. Logothetis and A. Haigh, *Qual. Reli. Eng. Int.*, **4**, 159 (1988).

30. G. R. Moradi, J. Ahmadpour, M. Nazari and F. Yaripour, *Ind. Eng. Chem. Res.*, **47**, 7672 (2008).

31. G. R. Moradi, R. Ghanei and F. Yaripuor, *Int. J. Chem. React. Eng.*, **4**, 14 (2007).

32. G. R. Moradi, M. Nazari and F. Yaripour, *Chem. Eng. J.*, **140**, 255 (2008).

33. Z. Ivorad and R. Lazic, *Design of Experiments in Chemical Engineering*, Wiley-VCH Verlag GmbH & Co. KGaA, Weinheim, Germany, ISBN 3-527-31142-4 (2004).